Available online at www.sciencedirect.com
SCIENCE DIRECT®
ELSEVIER
Nuclear Instruments and Methods in Physics Research A 499 (2003) 480–488
NUCLEAR INSTRUMENTS & METHODS IN PHYSICS RESEARCH Section A
www.elsevier.com/locate/nima

PHENIX magnet system

S.H. Aronson[a], J. Bowers[b], J. Chiba[c], G. Danby[a], A. Drees[d], O. Fackler[b], A. Franz[a,*], J.P. Freidberg[e], W. Guryn[a], A. Harvey[b], T. Ichihara[f], J. Jackson[a], R. Jayakumar[e], S. Kahn[a], V. Kashikhin[g], P.J. Kroon[a], M. Libkind[b], M.D. Marx[d], W.Z. Meng[a], F. Messer[d], S. Migluolio[e], I.D. Ojha[h], R. Prigl[a], G. Riabov[i], R. Ruggiero[a], N. Saito[f], R. Schleuter[j], Y. Severgin[g], A. Shajii[e], V. Shangin[g], T.K. Shea[a], W.E. Sondheim[k], K.H. Tanaka[c], R. Thern[a], J.H. Thomas[b], V. Vasiliev[g], C. Velissaris[l], R. Yamamoto[b]

[a] *Brookhaven National Laboratory, Upton, NY 11973-5000, USA*
[b] *Lawrence Livermore National Laboratory, Livermore, CA 94550, USA*
[c] *KEK, High Energy Accelerator Research Organization, Tsukuba-shi, Ibaraki-ken 305-0801, Japan*
[d] *Department of Physics and Astronomy, State University of New York at Stony Brook, Stony Brook, Stony Brook, NY 11794, USA*
[e] *Plasma Science and Fusion Center, Massachusetts Institute of Technology, Cambridge, MA 02139, USA*
[f] *RIKEN, The Institute of Physical and Chemical Research, Wako, Saitama 351-0198, Japan*
[g] *Efremov Institute for Electrophysical Research, St. Petersburg, Russia*
[h] *Vanderbilt University, Nashville, TN 37235, USA*
[i] *Petersberg Nuclear Physics Institute, Gatchina, Russia*
[j] *Lawrence Berkeley National Laboratory, Berkeley, CA 94720, USA*
[k] *Los Alamos National Laboratory, Los Alamos, NM 87545, USA*
[l] *New Mexico State University, Las Cruces, NM 88003, USA*

The PHENIX collaboration

Abstract

The PHENIX magnet system is composed of three spectrometer magnets with warm iron yokes and water-cooled copper coils. The Central Magnet (CM) is energized by two pairs of concentric coils and provides a field around the interaction vertex that is parallel to the beam. This allows momentum analysis of charged particles in the polar angle range from 70° to 110°. The north and south Muon Magnets (MMN and MMS) use solenoid coils to produce a radial magnetic field for muon analysis. They each cover a pseudorapidity interval of 1.1–2.3 and full azimuth. The coils are wound on cylindrical surfaces at the end of large tapered pistons. Each of the three magnets provides a field integral of about 0.8 T-m. The physical and operating parameters of the magnets and their coils are given along with a description of the magnetic fields generated. The geometric, thermal and magnetic analysis leading to the coil design is discussed. The magnetic volumes of the PHENIX magnets are very large and complex, so a new technique was developed to map the fields based on surface measurements of a single field component using single axis Hall probes

*Corresponding author. Tel.: +1-631-344-4750; fax: +1-631-344-3253.
E-mail address: afranz@bnl.gov (A. Franz).

0168-9002/03/$ - see front matter
PII: S0168-9002(02)01951-4

mounted on a rotating frame. A discussion of the performance of the CM during the first year of PHENIX running is given.

PACS: 07.55.Db; 25.75.−q; 29.30.Aj

Keywords: Magnet; Solenoid; Field mapping; Spectrometer; Heavy ions; RHIC

1. Introduction

The PHENIX detector [1] at the Relativistic Heavy Ion Collider (RHIC) is designed to perform a broad study of A–A, p–A and p–p collisions to investigate nuclear matter under extreme conditions. The PHENIX detector comprises four spectrometers, each subtending about one steradian of solid angle and each extending to about 6 m from the collision point. The central spectrometers measure electrons, photons and hadrons with excellent resolution and a pair of forward spectrometers provide excellent resolution for muon pairs. Momentum analysis of charged particles in these spectrometers thus requires large magnetic field volumes. The magnets, developed for PHENIX primarily by Brookhaven National Laboratory (BNL), Los Alamos National Laboratory (LANL), Lawrence Livermore National Laboratory (LLNL), the St. Petersburg Nuclear Physics Institute (Gatchina, Russia) and the Efremov Institute for Electrophysical Research (St. Petersburg, Russia) are shown in section in Fig. 1. Fabrication and assembly was performed at Izhora Steel Works (St. Petersburg), Mitsubishi Electric Company (Kobe, Japan), Tokin Corporation (Sendai, Japan) and BNL. A vertical cutaway view of the central and north muon magnets is shown in Fig. 2 in which the position of the magnet coils is indicated. Table 1 lists some of the

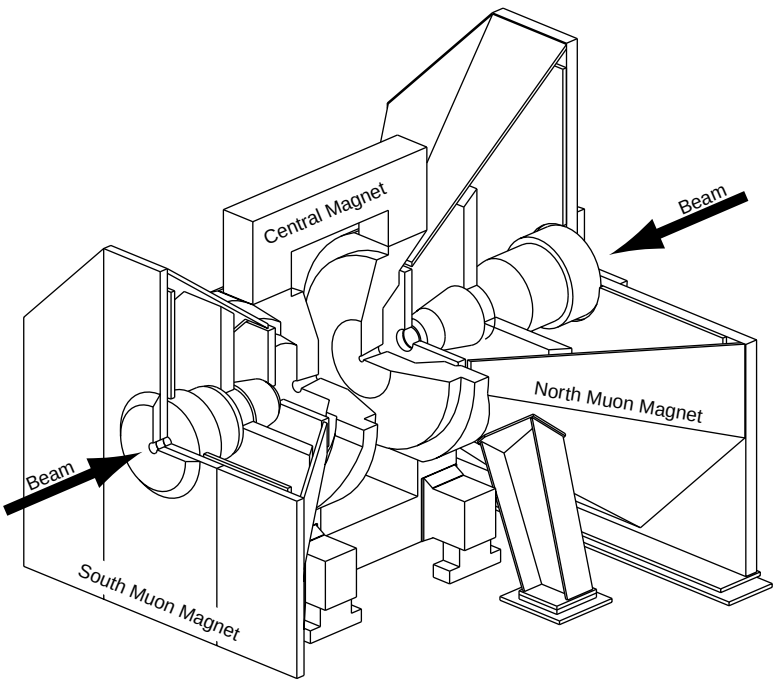

Fig. 1. Line drawings of the PHENIX magnets, shown in perspective and cut away to show the interior structures. Arrows indicate the beam line of the colliding beams in RHIC.

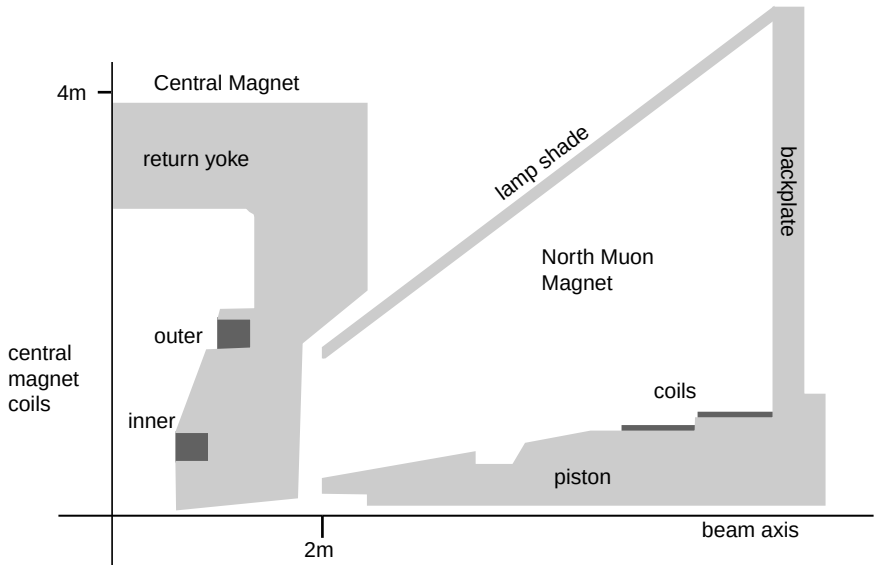

Fig. 2. Vertical cutaway drawing of central and north muon magnets showing the coil positions for both magnets.

basic parameters of the three magnets. The parameters of Central Magnet (CM) are also shown with only the outer coils present. This was the configuration during the first year of running.

In subsequent sections we present more detailed descriptions of the three magnets, including requirements, field characteristics and operations.

2. Central magnet

2.1. Specification and design

The primary physics-driven requirements for the CM design were:

(i) No mass in the apertures of the central spectrometer arms to minimize interactions and multiple scattering of particles produced in the primary collision and to minimize albedo from the magnet poles.

(ii) Dense material near the collision point in the apertures of the north and south muon spectrometers to serve as hadron absorbers. The CM pole tips serve as the hadron absorbers for the muon spectrometers. They comprise 60 cm of low-carbon steel and 20 cm of brass (about 4.9 nuclear interaction lengths).

(iii) Reasonably uniform field that could be mapped to a precision in the field integral of about 2 parts in 10^3.

(iv) Control over the radial field distribution to allow creation of a "zero-field" region near $R = 0$.

(v) Minimal field integral for the region $R >$ 200 cm, the radius of the Drift Chamber (DC). In particular the field integral in the Ring Imaging Cherenkov Counter (RICH) (2.4 m $< R <$ 4.0 m) was required to be less than 100 G-m. This is to minimize the smearing of the rings associated with low momentum electrons. Field in the region of the photomultiplier tubes of the RICH and the Electromagnetic Calorimeter (EMCal) was also required to be low.

(vi) The magnet must be easily moveable to allow access to detector components for commissioning, maintenance and replacement.

The resulting design (see Fig. 1) and fabrication drawings were done at LLNL. All three magnets were designed using the magnetic field simulation

Table 1
PHENIX magnet parameters

Parameter	CM	CM	MMN	MMS
CM coils	Inner and Outer	Outer only		
Field configuration	Axial	Axial	Radial	Radial
Field integral	0.43–1.15	0.78	0.72	0.72
(T-m)	($\Theta = 90°$)	($\Theta = 90°$)	($\Theta = 15°$)	($\Theta = 15°$)
Wt. (metric tons)	421	421	355	248
Pseudorapidity coverage	$-0.35 < \eta < 0.35$	$-0.35 < \eta < 0.35$	$1.1 < \eta < 2.4$	$-2.2 < \eta < -1.1$
Polar angle coverage (°)	$70 < \Theta < 110$	$70 < \Theta < 110$	$10 < \Theta < 37$	$12 < \Theta < 37$
Amp-turns	1,082,000	496,000	600,000	786,000
Power (kW)	928	600	225	342
Average coil temp. (°C)	23.8 (I)/32.1(O)	32.1	25.6–27.1	28.1–30.2

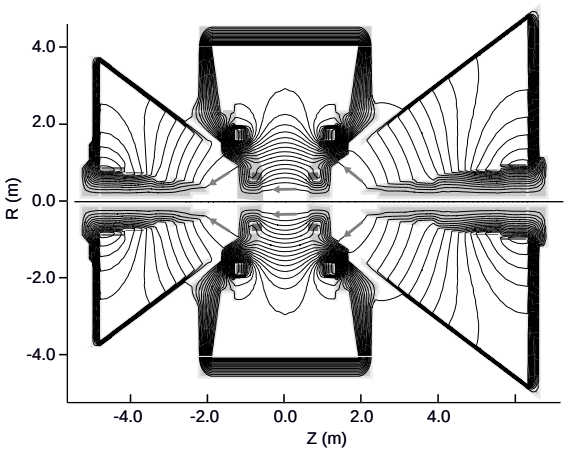

Fig. 3. CM and MM field lines shown on a cutaway drawing of the PHENIX magnets. The beams travel along the $R = 0$-axis in this figure and collide at $R = Z = 0$. Arrows indicate the field direction.

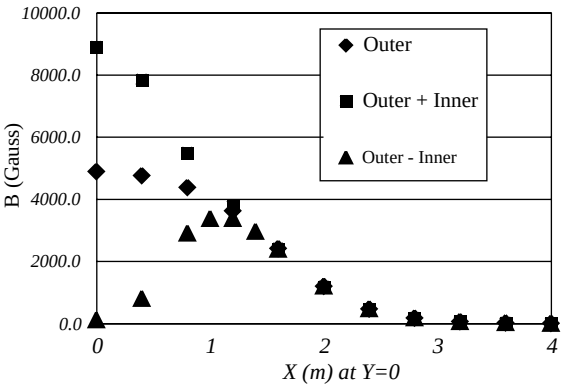

Fig. 4. Total field strength $B_{\mathrm{Mod}}(R)$ vs. R for + (Outer), ++ (Outer + Inner), and + − (Outer − Inner) field configurations.

programs, PE2D and TOSCA,[1] to help set the parameters for the complete mechanical design for the magnet steel and the electrical design for the coils. The final design entailed a number of compromises between the physics requirements listed above. For example, the first requirement dictated an open axial field geometry, with no solenoid coil in the path of the secondaries. The resulting field, depicted in Fig. 3, is therefore not as uniform as a solenoid. The mapping method and comparisons with detailed 3D field calculations using TOSCA are discussed in Section 4.

[1] Vector Fields Limited, 24 Bankside, Kidlington, Oxford OX5 IJE, England.

The fourth requirement was addressed by a design with two sets of circular coils set in the CM polefaces as seen in Fig. 2. These coils can be run with the fields for the two coil sets adding (the "++" configuration) or bucking ("+−"). During the initial operation of PHENIX only the outer coils were in place (the "+" configuration). Fig. 4 shows the total field component B_{Mod} as a function of R at the $\Theta = 0$ symmetry plane of the CM for these configurations.

There is a range of choices for the relative currents in the two sets of coils. The +− field plotted in Fig. 4 employs currents that give approximately zero field integral in the range $0 < R < 50$ cm. This feature will be used in conjunction with detectors in this radial space that must be efficient for very low momentum

electrons. Such electrons are a significant source of background in the measurement of e^+e^- pairs produced at RHIC. This measurement is a key ingredient in the PHENIX physics program. Also the ++ field plotted in Fig. 4, used with an upgraded charged particle tracking system, will improve the momentum resolution.

2.2. Fabrication and assembly

The yoke of the CM (and that of the MMN, discussed below) was fabricated at the Izhora Steel Works in St. Petersburg from low-carbon steel (the Russian equivalent of 1006 steel) forgings and hot-rolled plate. 1006 steel has a maximum carbon content of 0.08%. Trial assembly for fit was performed successfully at Izhora, but the yoke was not married to the coils until final assembly at BNL. Quality Assurance (QA) for permeability and uniformity of the steel at the factory in Russia could therefore not rely on magnetic excitation tests. QA was done on the magnet components with a combination of X-ray and ultrasonic inspection. Chemical analysis on melt samples was performed at Izhora and at LLNL. The results from these tests were integrated into the models used to design the magnets to verify that the steel properties would meet the design requirements. The results were excellent, as confirmed by powering and mapping the CM at BNL.

The outer coils of the CM were fabricated in Japan at Tokin Corporation [2]. Each coil pack comprises six bifilar wound double pancakes made with 20.3 mm × 20.3 mm copper conductor insulated with fiberglass reinforced epoxy. The outer coils consist of two assemblies each having 144 turns. The coils are water-cooled via a 12.8-mm hole in the conductor. The full current testing of two coil assemblies was performed at KEK before the shipment to BNL. Mapping of and performance experience with the CM is all with only the outer coils installed. The inner coils will be fabricated and installed (and the magnet re-mapped) within the next two years. The inner coils consist of two assemblies each having 120 turns.

Table 2
CM power supply specifications

Parameter	Specification
Output power (kW)	900 (2000 A, 450 V DC)
Control mode	Current control with voltage limit
Input voltage	480 VAC, 60 Hz, 3-phase
Output voltage ripple	1%
Long-term reproducibility	0.1% (1 year)
Stability	0.1% 1 min to 1 year
Remote control & status	RS 422

2.3. Performance and operations

The CM is powered with an Inverpower power supply having the specifications shown in Table 2.

During the Summer of 2000 the CM was operated continuously for over a month at either half-field or full field. The magnet was controlled by a graphical user interface, which sent the appropriate line commands to the power supply. All necessary parameters, such as ramp rate, target current, etc., are also controlled this way. The field was monitored with a set of fixed Hall probes that were read out into the event data stream. The same system will be used when the muon magnets are brought into routine operation.

3. Muon magnets

3.1. Specification and design

The primary physics drivers of the muon magnet design were as follows:

(i) Large acceptance to maximize the acceptance for muon pair events with full azimuthal coverage and minimum polar angle as close as possible to the beam direction. The maximum polar angle as large as practical, given the constraints of the collision hall on the muon spectrometers' acceptance.
(ii) Minimal effect on RHIC circulating beams from muon magnet fields.
(iii) Reasonably uniform field that could be mapped to a precision in the field integral of about 1 part in 10^2.

The basic design, shown in Fig. 1 with major parameters listed in Table 1, is a unique spectrometer

magnet, which produces a radial magnetic field. The central iron "piston" is surrounded at its base with a coil and defines the minimum polar angle of the spectrometer. The rest of the iron yoke consists of an 8-sided "lampshade", which defines the maximum polar angle and a back plate that connects the piston and lampshade. The resulting radial magnetic field (see Fig. 3) has an integral that is roughly proportional to the polar angle Θ. This is a nice feature, since the typical momentum of muons accepted by the spectrometer is also roughly proportional to Θ. The azimuthal (ϕ) aperture is 2π, except for two relatively thin fins that stabilize the end of the piston from below. The forward end of each magnet is open to the rear of a CM pole, which forms the hadron absorber for the muon spectrometer. A low-carbon steel back plate closes the back end of each magnet. The back plate is 30 cm thick on MMN and 20 cm on MMS. This back plate, in turn, forms the first of several layers of absorber, each followed by Iarocci tube planes. This stack of steel and proportional tubes, called the muon identifier, is used to identify and trigger on muons and is described elsewhere in this issue [3]. It is interesting to note that the MMN back plate involved the rolling and machining of the largest steel plates (5 m wide, 34 cm thick, 120 ton) ever fabricated in Russia, possibly in the world.

Because of the shape of the field, charged particles trace out helix-like trajectories, moving in ϕ at approximately constant Θ. The muon tracking is accomplished with three cathode strip chambers mounted on and in each muon magnet and described elsewhere in this issue [3]. The two muon magnets, MMN and MMS are somewhat different in detail. MMN is the full length along the beam line allowed between the pole of the CM and the muon identifier subsystem near the wall of the collision hall. Its piston defines a 10° minimum polar angle. MMN is fixed in the hall. MMS is mobile in order to allow access and mobility for other detector components. As a result of the detector and hall geometry it is 1.5 m shorter than MMN, and in order to achieve comparable performance ($\int B\,\mathrm{dl}$) to MMN, the MMS was designed to have a larger piston angle. Due to the saturation of the steel in a narrower piston, the MMS piston angle was increased to 12°. Because of its greater length and smaller piston angle, MMN has somewhat better acceptance for low-mass muon pairs (e.g. $\phi \to \mu^+\mu^-$) and somewhat better mass resolution for high mass muon pairs (e.g. $\Upsilon \to \mu^+\mu^-$). Table 3 compares the physics performance of MMN and MMS. The detailed designs for MMN and MMS were also carried out at LLNL.

Table 3
Muon magnet physics performance

	MMN	MMS
Acceptance of $\phi \to \mu^+\mu^-$	0.0058	0.0023
RMS mass resolution for $\Upsilon \to \mu^+\mu^-$ (MeV/c^2)	190	240

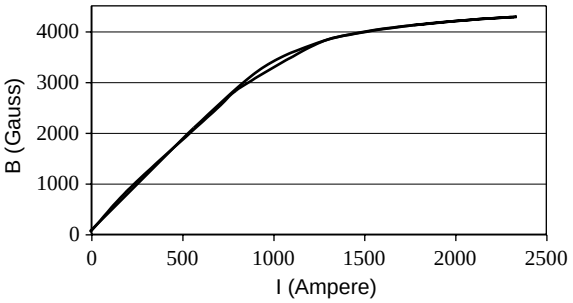

Fig. 5. B vs. I for MMS. The two lines represent the hysteris loop for increasing and decreasing the magnet current.

3.2. Fabrication and assembly

The MMN yoke was fabricated at the Izhora Steel Works in St. Petersburg and the coils for MMN were fabricated at Mitsubishi Electric Co. in Japan. Mitsubishi also fabricated the yoke and coils for MMS. Both magnets performed according to calculations based on the design. Fig. 5 shows the magnetic performance of MMS. The magnetic field was measured at the front of the piston and approximately 50 cm from the center line.

3.3. Performance and operations

Power supplies for MMN and MMS are listed in Table 1. Although both magnets were operated for mapping purposes (see Section 4), MMN has not yet seen service in physics running as of this writing. MMS began operation in the physics run

starting in June 2001. MMN is expected to operate for the first time for physics in the Fall of 2002. After installation of all tracking chambers the MMS was successfully tested in place and will be operated using the same graphical user interface as the CM. All magnets contain permanent Hall probes to monitor the stability of the field during operation. The probes are read out by the PHENIX slow control system and are archived in the run database [4].

4. Mapping and field computation

A number of methods were considered to produce field maps for the large, irregularly shaped field volumes in CM, MMN and MMS:

(i) Conventional 3D maps obtained from the direct measurement of multiple field components at each of a large number of points on a regular grid filling the field volume.
(ii) Maps computed from measurements of a single field component at points on a closed surface containing the useful field volume using Laplace's equation.
(iii) Maps calculated from a 3D field simulation program (TOSCA), using detailed geometry and steel properties from the design and spot-checked with a limited number of field measurements.

Several field maps had to be obtained with various combinations of currents through the three detector magnets, which disfavored the time-consuming direct measurement of the field in the region of interest. After successful demonstrations of the surface mapping technique using wire loop models as input, it was decided to use this technique in combination with a limited number of measurements in the volume. The volume measurements were needed to check both the solutions to Laplace's equation and the TOSCA simulations. The results for the CM were, in brief, that an accuracy of one part in 10^3 was achieved using method 2. In addition it was found that the TOSCA simulation was accurate enough to use in place of the field computed from the surface map in the case where both muon magnets are off. TOSCA simulations of CM plus MMN and/or MMS are considerably less accurate mainly due to the difficulties in combining two magnets with very different geometries into a single model.

Details of the surface mapping method and comparison of its output to both volume measurements and simulations are given in subsequent sections.

4.1. Surface mapping

The surface mapping method provides a calculation of the magnetic field in a region that is free of magnetic field sources, based on field measurements performed only at points on the surface of that region. One approach is to use the Finite Element technique where the magnetic scalar potential Φ is a solution of the Laplace equation,

$$\nabla^2\Phi = 0 \tag{1}$$

Φ is obtained on a calculation grid inside the volume by mapping the measured boundary conditions to the grid. An alternative to the evaluation of the potential Φ in the volume is the use of Green's theorem

$$\sigma\Phi = \int \Phi'\mathbf{n}' \cdot \nabla'\mathbf{G}\, d\mathbf{S}' - \int \mathbf{G}\mathbf{n}' \cdot \nabla'\mathbf{V}'\, d\mathbf{S}' \tag{2}$$

where

$$\sigma = \begin{cases} 1: & \text{interior observation point,} \\ 1/2: & \text{surface observation point,} \\ 0: & \text{exterior observation point} \end{cases}$$

and

$$G = -\frac{1}{4\pi}\frac{1}{|\mathbf{r}' - \mathbf{r}|} \tag{3}$$

is the infinite space Green's function. The prime denotes the integration surface **S**. By choosing an observation point on the surface ($\sigma = 1/2$), the potential $\Phi(S) \equiv \Phi_S$ can be found from a measurement of the normal field component B_n on S. With B_n and Φ_S known, the magnetic field in the interior region ($\sigma = 1$) is found by evaluating the resulting surface integrals

$$\mathbf{B}(\mathbf{r}) = \int \Phi'_S \nabla\left(\frac{\partial \mathbf{G}}{\partial \mathbf{n}'}\right) d\mathbf{S}' - \int \mathbf{B}'_n \nabla\mathbf{G}\, d\mathbf{S}'. \tag{4}$$

Thus the field in the volume can be calculated from the potential and normal field component on the surface, and gradients of the Green's function which can be obtained analytically. Compared to the Finite Element method, the 3-D volume problem for $\Phi(\mathbf{r})$ has been reduced to a 2-D problem for $\Phi(S)$. In the PHENIX magnets, as would be the case in most other detector magnets, the field map is obtained by rotating a mapping frame about the magnet axis, which makes the mapping surfaces azimuthally symmetric. In this case the field and potential can be expanded in Fourier series with respect to the azimuthal angle, and the problem of solving for the potential on the surface (Eq. (2)) decouples into a set of 1-D equations for each of the Fourier harmonics. Based on this method, we developed a code for field reconstruction and successfully tested it with a model field created by a large number of current loops to provide a field shape close to that of the CM. Also we are using the above method to reconstruct the field from surface measurements.

4.2. The setup

The mapping fixtures consisted of aluminum plates with a large number of mounting holes for Hall probes along the perimeter and along several radial lines in the interior. The plates were fixed to aluminum support structures that could be rotated about the magnet axis. The CM mapping fixture was rotated by a nonmagnetic ultrasonic motor (REF. USR60, Fukoku Co. Ltd. Japan, sold by Asami Boeki Co., Ltd., Osaka, Japan). The MMN

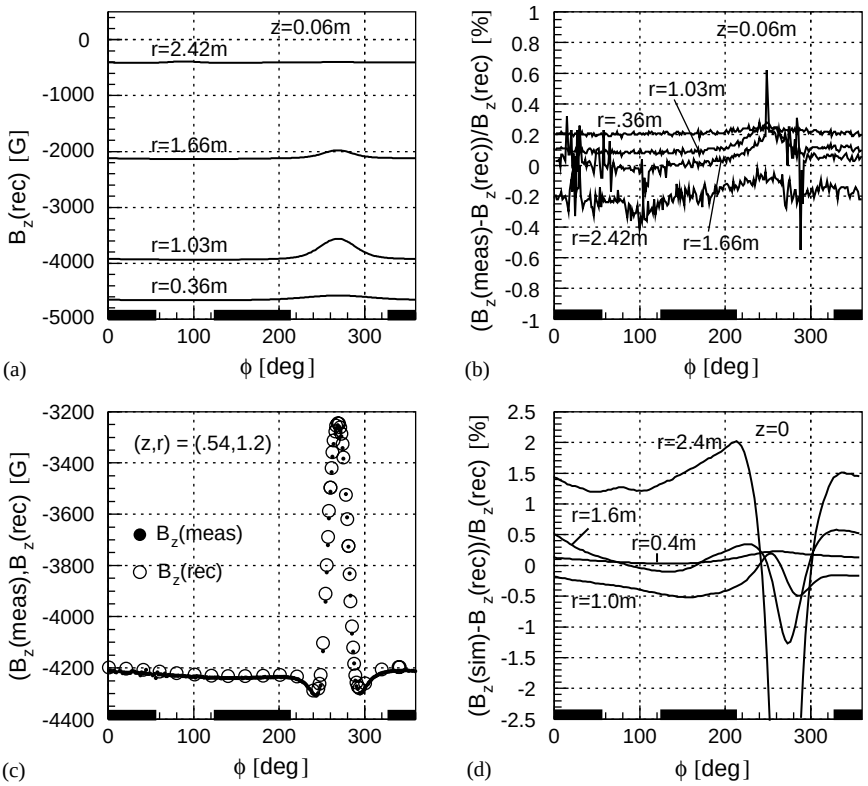

Fig. 6. (a) Reconstructed B_z values as a function of ϕ for various radii; (b) percentile difference between measured and reconstructed B_z values as a function of ϕ for various radii; (c) measured and reconstructed B_z values for a single probe as a function of ϕ and (d) percentile difference between simulated and reconstructed B_z values as a function of ϕ for various radii. The solid lines along the ϕ-axis denote the acceptance of the PHENIX central arms.

and MMS fixtures were rotated by stepping motors mounted outside the magnets. The angle of rotation was read out by optical encoders (K25-P-W-1024-N, BEI Sensors & Motion Systems Company, Sylmar, CA). Measurements in the CM were taken in about 1.4° steps, 256 measurements for a full rotation. Total measurement time for one map was about 4 h. For MMS the frames were rotated in 2.8° steps, but a full turn could not be completed due to interference with the leads to the magnet coils. Given the 8-fold symmetry in azimuth of MMS, the loss in azimuthal coverage was preferred over the substantial loss in coverage of the (R, Z)-plane that would have been required to clear the leads.

The CM frame was instrumented with 288 Hall probes, arranged in 16 chains around the perimeter of the mapping fixture and along radial lines in the interior. Each chain had a precision resistor (10 Ω) to monitor the Hall current of approximately 100 mA through the 18 probes in the chain. The Hall probe voltages were read out using a 400-channel Keithley 7002 multiplexer connected to a Keithley 2000, $6\frac{1}{2}$-digit multimeter. A Gateway PC, used for readout and data storage, was connected to the multiplexer though a GPIB bus. The Hall probes were fabricated, hardwired to a 100 × output voltage amplifier, and then calibrated at the Scientific Technical Center CYCLONE, St. Petersburg. The probes were of very good quality with output voltage temperature coefficients of typically 0.001%/°C or less, stable offsets and small planar Hall coefficients. After assembly of the chains at BNL, the calibration of the probes was checked for a few field values in a long dipole magnet, and good agreement with the calibrations done in Russia was found. For the chains used in MMS, a small correction had to be applied for a current drop along the chains caused by the relatively low input impedance of 100 kΩ of the Hall voltage amplifiers. In those chains a second 10 Ω resistor was added to measure the Hall current on both ends of the chain. For the probes used in the CM, an improved amplifier circuit was used and the current drop was negligible.

In addition to the probes on the mapping frames, permanent probes were mounted in the magnets and read out together with the map data stream for future field normalization.

4.3. CM surface mapping results and comparison with simulation

The field map reconstructed from measurements on the surface was compared to the measurements inside the mapped volume, see Fig. 6(a)–(c). The reconstructed values agree with the direct measurements within a few tenths of 1% for single point measurements in the high field region, and even better for the $\int B\,\mathrm{d}L$, along the lines of typical particle trajectories.

The field map of the CM with the muon magnets off was compared to a TOSCA simulation of the CM only. This allowed an optimization of the mesh in the TOSCA model with respect to the CM geometry, particularly the shape of the return yoke and the vertical slot for the inner coil current leads, which break the azimuthal symmetry. Typical differences between simulation and reconstruction are shown in Fig. 6(d). The simulation is not as accurate as the reconstruction, particularly near $\phi = 270°$, the location of vertical slots in the poles for the power bus lines to the inner coils. However, this region is outside the acceptance of the CM detector arms and field integrals along typical particle trajectories agree with the reconstructed map to 0.3% or better. Thus the simulation map satisfies the specification of 0.5% accuracy for momentum reconstruction.

The comparison of reconstructed field maps in the muon magnets with measurements inside the mapping region and with simulations is in progress.

Acknowledgements

We acknowledge support from the Department of Energy (USA).

References

[1] K. Adcox, PHENIX detector overview, Nucl. Instr. and Meth. A (2003), this issue.
[2] R.M. Yamamoto, et al., IEEE Trans. Magn. 32 (1996) 2140.
[3] H. Akikawa, et al., PHENIX muon arms, Nucl. Instr. and Meth. A (2003), this issue.
[4] S.S. Adler, et al., PHENIX on-line systems, Nucl. Instr. and Meth. A (2003), this issue.